J. Fluid Mech. (1983), *vol.* 134, *pp.* 431–458
Printed in Great Britain

The 'whistler-nozzle' phenomenon

By A. K. M. F. HUSSAIN AND M. A. Z. HASAN
Department of Mechanical Engineering, University of Houston, Texas 77004

(Received 14 December 1982 and in revised form 10 May 1983)

The 'whistler nozzle' is a simple device which can induce jet self-excitations of controllable amplitudes and frequencies and appears highly promising for many applications involving turbulent transport, combustion and aerodynamic noise. This paper documents the characteristics of this curious phenomenon for different values of the controlling parameters and explains the phenomenon. It is shown that the whistler excitation results from the coupling of two independent resonance mechanisms: shear-layer tone resulting from the impingement of the pipe-exit shear layer on the collar lip, and organ-pipe resonance of the pipe nozzle. The crucial role of the shear-layer tone in driving the organ-pipe resonance is proven by reproducing the event in pipe–ring and pipe–hole configurations in the absence of the collar. It is also shown that this phenomenon is strongest when the self-excitation frequency matches the 'preferred mode' of the jet.

The 'whistler-nozzle' phenomenon occurs for both laminar and turbulent initial boundary layers; the excitation can be induced without the pipe nozzle (say, by ring or hole tone) when the exit flow is laminar but not when it is turbulent. Unlike the shear-layer tone and jet tone phenomena, where successive stages overlap, adjacent stages of the whistler-nozzle excitation are separated by 'dead zones' where the conditions for both resonance mechanisms cannot be simultaneously met. Also, unlike the shear-layer and jet tones, the whistler frequency cannot be varied continuously by changing the speed. Since the phenomenon is the coupling of two resonance mechanisms, the frequency data appear to defy a simple nondimensional representation for the entire range of its operation. Reasonable collapse of data is achieved, however, when the exit momentum thickness is used as a lengthscale, thus emphasizing the role of the shear-layer tone in the phenomenon.

1. Introduction

In an attempt to explore turbulence augmentation and suppression as well as the role of the large-scale coherent structures, and their interactions like tearing and pairing, in jet noise and mixing, we were interested in methods of inducing controlled excitations in the jet. The 'whistler nozzle' presented itself as an attractive possibility because of its amazingly simple configuration, requirement of no external power, and ability to induce self-sustained excitation of controllable amplitudes and frequencies over wide ranges.

The device consists of a round tailpipe attached to the downstream end of a jet nozzle and an axisymmetric collar sliding over the pipe (figure 1*a*). As the collar is pulled downstream (i.e. the collar length L_c projecting beyond the pipe is increased), a loud pure tone abruptly appears; (the tone is audible in air at velocities as low as 15 m s^{-1}). This is called the first stage. With increasing L_c, the tone increases in amplitude, reaches a maximum, decreases and then disappears. With a further increase in L_c, the tone reappears. This is the second stage, and so on. The tone

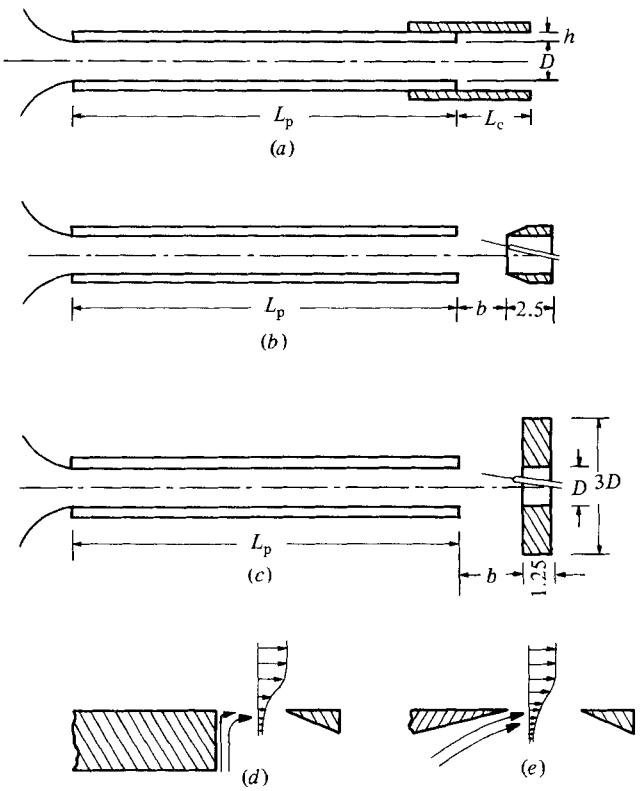

FIGURE 1. Schematics of different experimental configurations: (*a*) pipe–collar; (*b*) pipe–ring; (*c*) pipe–hole; (*d*) transverse entrainment at lip; (*e*) nearly parallel entrainment at lip. All dimensions are in cm.

frequency and amplitude depend on the pipe-nozzle length L_p, collar length L_c, step height h (i.e. the difference between the inner radii of the nozzle and the collar), jet exit speed U_e, and jet diameter D.

Hill & Greene (1977) appear to be the first to have discovered whistler-nozzle excitation, but they were unable to explain the phenomenon or find any relationship between the controlling parameters. The motivation for the present study was to document the whistler-nozzle behaviour as a function of the controlling parameters, to explain the phenomenon and to validate the explanation via additional experiments in modified configurations (figures 1*b*, *c*) without the collar. The phenomenon was explored in low-speed axisymmetric air jet facilities available in our laboratory. The effects of the self-sustained excitation on the axisymmetric free jet emerging from the whistler nozzle have been discussed previously (see Hasan & Hussain 1982, hereinafter referenced as HH). Measurements up to 60 diameters showed that the whistler-nozzle excitation produces a large increase in the turbulence intensity in the near field of the jet, while it increases the spread and decay rate for the entire x-range of measurement. For further details see HH, which complements the results reported here.

The shear-layer tone phenomenon

If an object intercepts a laminar free shear layer, the shear layer can be set into oscillation, depending on the speed U_e and the distance b of the object from the lip. The oscillation can produce discrete audible tones like the jet tone at even fairly low speeds, especially with a sharp edge. As b is increased from zero, a tone abruptly

appears, and the frequency of the tone decreases with increasing b. With further increase in b, the tone jumps back to a higher frequency. The average frequency remains the same at successive stages and is the instability frequency of the shear layer stabilized by feedback from the impinging edge. The frequencies in the different stages show collapse when non-dimensionalized by U_e and the exit momentum thickness θ_e. For further details, see Hussain & Zaman (1978, hereinafter referenced as HZ).

2. Apparatus and procedure

The experiments have been carried out in two axisymmetric air-jet facilities with nozzle diameters $D = 2.54$ and 7.62 cm. The 2.54 cm jet facility has been described by Zaman & Hussain (1980). The $D = 2.54$ cm pipe is attached to the settling chamber via an ASME nozzle (see HH). Data with the 7.62 cm nozzle were obtained in a large jet of 27 cm diameter. The transition to the $D = 7.62$ cm pipe occurs through an ASME nozzle. Additional details of the facility were given by Husain & Hussain (1979).

The centreline longitudinal turbulence intensity at the inlet end of the pipe is about 0.2 % for each facility. For the 2.54 cm jet, data were taken with six different values of L_p (7.62, 15.24, 30.48, 45.72, 60.96, and 91.44 cm) and two values of h (0.3175 and 0.635 cm). Unless otherwise stated, data presented for the 2.54 cm nozzle are for $U_e = 36$ m s^{-1} corresponding to the jet Reynolds number Re_D ($= U_e D/\nu$) of 6.2×10^4. For $D = 7.62$ cm, data were taken with two values of L_p (30.48 and 60.96 cm) at U_e values of 36, 45 and 60 m s^{-1}. The corresponding values of Re_D were 1.85×10^5, 2.3×10^5 and 3.1×10^5 respectively. For $D = 7.62$ cm, only one step height h ($= 0.635$ cm) was investigated.

A standard tungsten hot wire of 40 μm diameter, operated at an overheat ratio of 0.4 by a linearized (DISA) constant-temperature anemometer, was used to obtain the data. Most of the data were obtained with a backlash-free traversing mechanism operated by stepping motors, which were controlled on-line by the laboratory computer (HP2000S). The frequency spectra were obtained with a real-time spectrum analyzer (Spectrascope model SD335). The phase of the disturbance signal was measured with a PAR lock-in amplifier; the reference signal was obtained from the flow by bandpassing the velocity signal in the near field of the excited jet.

Note that the origin of the coordinates is located at the pipe-exit centre; x increases in the downstream direction and y increases radially.

3. Results and discussion

3.1. *General characteristics*

For the 2.54 cm nozzle, unless otherwise specified, data for two L_p values representing two distinctly different initial conditions (i.e. flow characteristics at the pipe exit) will be presented in this paper. These are, first, $L_p = 15.24$ cm, which has a laminar exit boundary layer, and, secondly, $L_p = 30.48$ cm, which has a transitional exit boundary layer. For $D = 2.54$ cm, data for longer pipes having turbulent exit boundary layers are not included because all the 7.62 cm diameter pipes have turbulent exit boundary layers.

Even though a large number of measures can be used to define the initial condition, the mean velocity and longitudinal fluctuation intensity profiles and the u-spectrum in the exit boundary layer can be regarded as adequate identifiers of the

(*a*)

L_p (cm)	h (cm)	$L_{c\,min}$ (cm)	$L_{c\,min}/\theta_e$
15.24	0.3175	0.381	17.47
15.24	0.635	0.762	34.95
30.48	0.3175	0.66	15.64
30.48	0.635	1.016	24.08
60.96	0.3175	0.8128	8.02
60.96	0.635	1.2192	12.02

(*b*)

U_e (m s^{-1})	L_p (cm)	D (cm)	h (cm)	$Q\left(=\frac{\omega_n}{\Delta\omega}\right)$	Stage
36	15.24	2.54	0.3175	32	I
	15.24	2.54	0.3175	14	II
	15.24	2.54	0.635	14	II
	30.48	2.54	0.3175	28	I
	30.48	2.54	0.3175	16	II
	30.48	2.54	0.635	31	I
	30.48	2.54	0.635	15	II
	60.96	2.54	0.3175	37	II
	60.96	2.54	0.635	32	II
36	30.48	7.62	0.635	10	I
60	30.48	7.62	0.635	12	II
60	60.96	7.62	0.635	14	I

TABLE 1. (*a*) $L_{c\,min}$ values of the whistler nozzle for $U_e = 36$ m s^{-1}, $D = 2.54$ cm. (*b*) Approximate values of Q for whistler-nozzle excitation.

initial condition. The initial conditions can be classified into four groups: laminar, nominally laminar, highly disturbed and fully developed turbulent (for details see Hussain 1981). Both laminar and nominally laminar cases, identified by the agreement of the mean velocity profile with the Blasius profile, are grouped together in this study and termed 'laminar' for the sake of simplicity. For initially turbulent boundary-layer cases, the mean velocity profile had the characteristic logarithmic and wake regions in the universal (U^+, y^+) coordinates, the wake strength agreed with that expected for the corresponding value of Re_θ (Coles 1962), the longitudinal velocity fluctuation intensity profile agreed with that of the flat plate, and the longitudinal velocity spectrum $\phi_u(f)$ was broadband (typically over the frequency range 0–4 kHz) without any spectral peaks.

Based on exploratory tests, the whistler-nozzle phenomenon was inferred by us to be an organ-pipe resonance of the pipe nozzle triggered by the shear-layer tone, which is produced by the impingement of the shear layer from the pipe exit on the collar lip. Detailed data discussed in the following further affirm our explanation.

(*a*) *Minimum collar length*

If the whistler phenomenon involves a shear-layer tone, then there should be a minimum collar length $L_{c\,min}$ below which no excitation will take place. This is typical of the shear-layer tone and the jet tone phenomena (HZ; Karamcheti *et al.* 1969; Rockwell & Naudascher 1979). The $L_{c\,min}$ value depends on L_p as well as h. Table 1 (*a*) shows the values of $L_{c\,min}$ for a few cases. With higher values of h, $L_{c\,min}$ increases, since the collar has to be longer in order for its lip to intercept the shear layer and thus induce the shear-layer tone via feedback. Note that, for the laminar

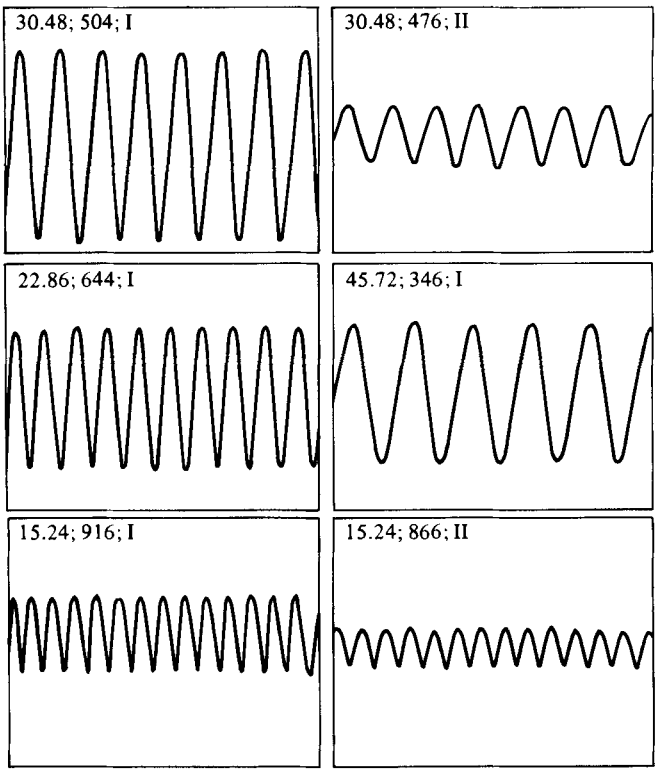

FIGURE 2. Longitudinal velocity $\tilde{u}(t)$-signal traces at the pipe-exit centreline for $U_e = 36$ m s^{-1} and $h = 0.3175$ cm. Inserts denote L_p(cm), f(Hz) and stage respectively.

case ($L_p = 15.24$ cm), the value of $L_{c\,min}$ is proportional to h. At a lower frequency (and hence longer wavelength), the shear-layer roll-up length should be longer and, thus, the length required for vortex impingement and feedback to sustain the shear-layer tone should be greater also. Since the excitation frequency decreases with increasing L_p, higher L_p gives higher $L_{c\,min}$ (table 1*a*).

(*b*) *Nature of the excitation*

Figure 2 shows hot-wire traces at the pipe-exit centreline for a few representative excitation cases covering different stages and L_p values for the 2.54 cm nozzle. The vertical and the horizontal scales for all the traces are identical. For each L_p, the trace corresponds to the value of L_c that produces the maximum excitation amplitude u'_e/U_e at the pipe-exit centreline. It is clear from figure 2 that the whistler nozzle induces a strong, stable sinusoidal surging of the flow for both laminar ($L_p < 15.24$ cm) and turbulent ($L_p > 30.48$ cm) boundary layers at the pipe exit. In the turbulent case ($L_p = 45.72$ cm), only the exit boundary layer is turbulent, but the core flow at the pipe exit is non-turbulent. Larger L_p values, in which the pipe exit flow is turbulent over the entire cross-section, also produce stable sinusoidal surging due to this self-excitation. It is apparent from the traces that the frequency decreases with increasing L_p, the second-stage frequency is somewhat lower than that in the first stage for a given U_e and L_p (explained later), the second-stage amplitude is lower than that in the first stage, and the peak excitation amplitude in the first stage is the largest for $L_p = 30.48$ cm and decreases for larger or smaller L_p.

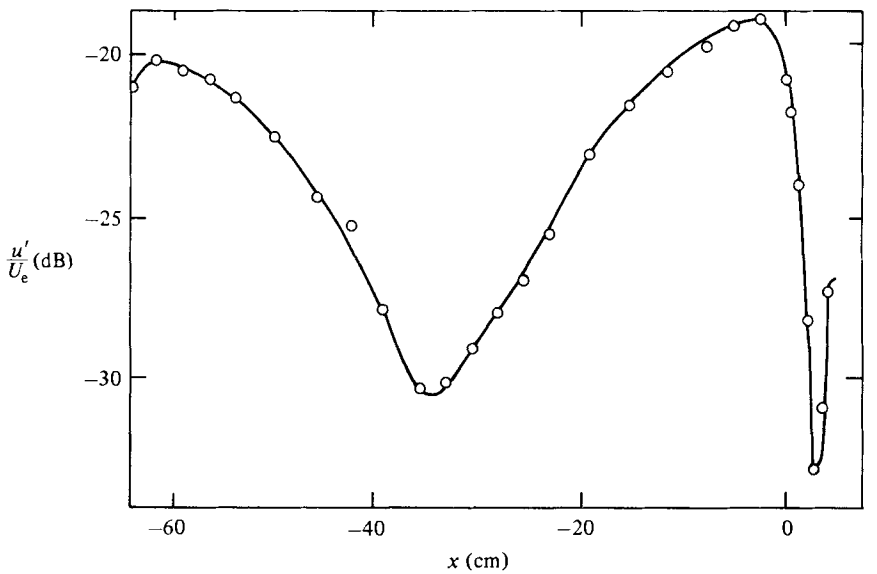

FIGURE 3. Longitudinal fluctuation intensity (u') distribution inside the pipe along the centreline for the first stage, $f = 244$ Hz, $D = 7.62$ cm, $L_p = 60.96$ cm and $U_e = 45$ m s^{-1}.

(c) *Organ-pipe excitation*

Even though a monotonic decrease of the self-excitation frequency f with increasing L_p suggests organ-pipe resonance of the nozzle, it was considered important to obtain direct evidence of this resonance. The u' distribution inside the pipe along the centreline at $U_e = 45$ m s^{-1} is shown in figure 3 for a halfwave mode in the first stage of excitation. The wavelength of a fullwave mode was found to be slightly larger than half of the halfwave mode. This is not unexpected, because the effective lengths for the two modes are likely to be different and should include corrections due to both the collar length L_c (Hasan & Hussain 1979) and the pipe diameter D (Kinsler & Frey 1962, p. 201). Data in figure 3 corresponds to the condition for which u'_e/U_e is the maximum. The vertical scale is logarithmic in order to accommodate large variations of the amplitude.

(d) *Axial evolution of the fundamental*

The axial evolution of fundamental amplitude u'_f on the centreline for a number of excitation situations involving different stages is shown in figures 4(a, b); x is non-dimensionalized by the jet diameter in figure 4(a) and by the corresponding acoustic wavelength λ_a in figure 4(b). In order to provide a meaningful basis for comparison between different cases, all data in figure 4 are for a fixed excitation amplitude u'_e/U_e of 3 %, achieved by adjusting L_c (see later). The collar-exit location for each curve is identified by a vertical hatched line in figure 4(a). Note that the data for $L_p = 60.96$ cm) ($D = 2.54$ cm) are also included. The centreline variation of u'_f depends on the relative contributions of the hydrodynamic (instability) wave and the acoustic wave. For an instability wave-dominated case, the axial distribution of u'_f should be initially exponential. The u'_f distribution is altered significantly from exponential when the contribution of the acoustic wave becomes comparable to or larger than that of the instability wave. This has been demonstrated by Rockwell & Schachenmann (1982, hereinafter referenced as RS) by using a one-dimensional model for an impinging jet on a cavity. Which form of oscillation will occur for a given

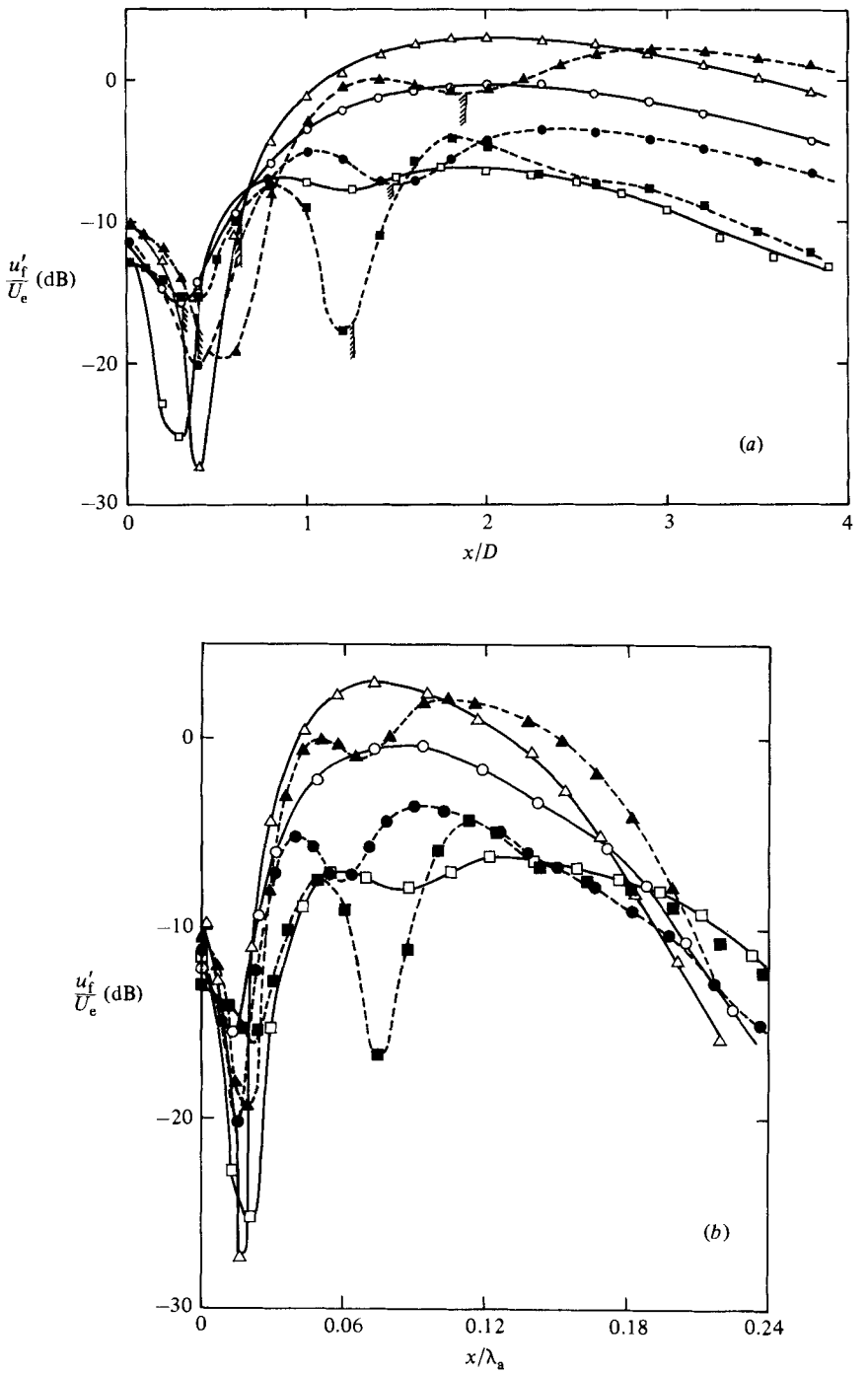

FIGURE 4. (*a*) Streamwise distribution of $u'_f(x/D)$ for $D = 2.54$ cm, $U_e = 36$ m s^{-1}, $h = 0.3175$ cm, $u'_e/U_e = 3\%$. The pipe lengths (cm), first-stage (open symbol) and second-stage (solid symbol) frequencies (Hz) are □, 15.24, 924, 820; △, 30.48, 480, 476; ○, 60.96, 536, 516. (*b*) The data of (*a*) as a function of x/λ_a; symbols as in (*a*).

self-sustained resonance condition is intimately connected with the 'quality factor' Q, which is directly related to the damping of the acoustic mode of the system. Typically, Q for a system is defined as $Q = \omega_n/\Delta\omega$, where ω_n is the resonance frequency (representing the maximum gain), and $\Delta\omega$ is the half-power bandwidth. For the whistler nozzle, the excitation amplitude varies with the collar length L_c, which also changes the frequency of excitation. Thus, from a plot showing the variation of u_e' with L_c (hence frequency), one should be able to calculate a crude Q-factor for the whistler nozzle. The estimated values of Q for different whistler-nozzle parameters are given in table 1 (*b*). A small value of Q should represent the case when the instability wave dominates the acoustic wave (see also RS). The high values of Q (in table 1 (*b*)) for the whistler nozzle suggest the presence of a strong acoustic wave.

In figure 4*a*, the amplitude u_f' drops sharply for all cases between $x/D = 0$ and $x/D = 0.8$ to a minimum value and then rises again. This drop in u_f' is predicted by RS's model for the case when the amplitudes of the acoustic and instability waves are comparable. The near-field dip was observed previously by Pfizenmaier (1973) and Hussain & Zaman (1975), even though this dip was surprisingly absent in the data of Crow & Champagne (1971). Note that the dip in u_f' distribution for different cases occurs at nearly the same location ($x/\lambda_a \approx 0.016$) when plotted against x/λ_a (figure 4*b*). In figure 4(*b*), the distance between the first and second dips gives an approximate measure of the disturbance wavelength λ. Based on this wavelength, the relationship between collar length and disturbance wavelength was found to be $L_c/\lambda = n - c$, where n is the stage of excitation and $c = 0.5$. The value of c varies between different impinging flow geometries. A summary of the L_c/λ values for different impinging shear layers is given by Ziada & Rockwell (1982).

(*e*) *Dependence on velocity*

Attempts were made to document the variation of the whistler excitation frequency with velocity. For a given L_c as the velocity was increased slowly, the whistler excitation appeared only for a small velocity range after which the tone disappeared with a further increase in U_e. For a few cases, the whistler excitation could be triggered again at a higher velocity. The variation of the excitation frequency with L_c is due to the fact that the effective length of the pipe–collar combination changes with L_c. However, for a fixed L_c, when U_e is changed, the corresponding shear-layer tone frequency does not match one of the organ-pipe mode frequencies. That is why, unlike the jet tone and shear-layer tone phenomena, whistler-nozzle excitation cannot be obtained for a fixed L_c at any arbitrary exit velocity.

3.2. *Frequency and amplitude variation with the collar length*

Perhaps the best demonstration of the underlying phenomenon in the whistler nozzle is the dependence of the excitation frequency f on L_c. Since the phenomenon is the coupling of two resonance mechanisms, i.e. the organ-pipe resonance and the shear-layer tone, the frequency jumps must also depend on L_p. The dependence of the excitation frequency and amplitude on L_c are demonstrated for some representative cases in figures 5 and 6. Figures 5(*a–c*) show the variation of f with L_c; figures 6(*a–c*) show the corresponding amplitudes. Only those spectral components with amplitudes within 45 dB of the highest peak for each L_p are included.

(*a*) *Laminar and transitional initial conditions*

Figures 5(*a*) and 6(*a*) cover data for $L_p = 15.24$ cm which has a laminar exit boundary layer. Figures 5(*b*) and 6(*b*) correspond to a transitional exit boundary

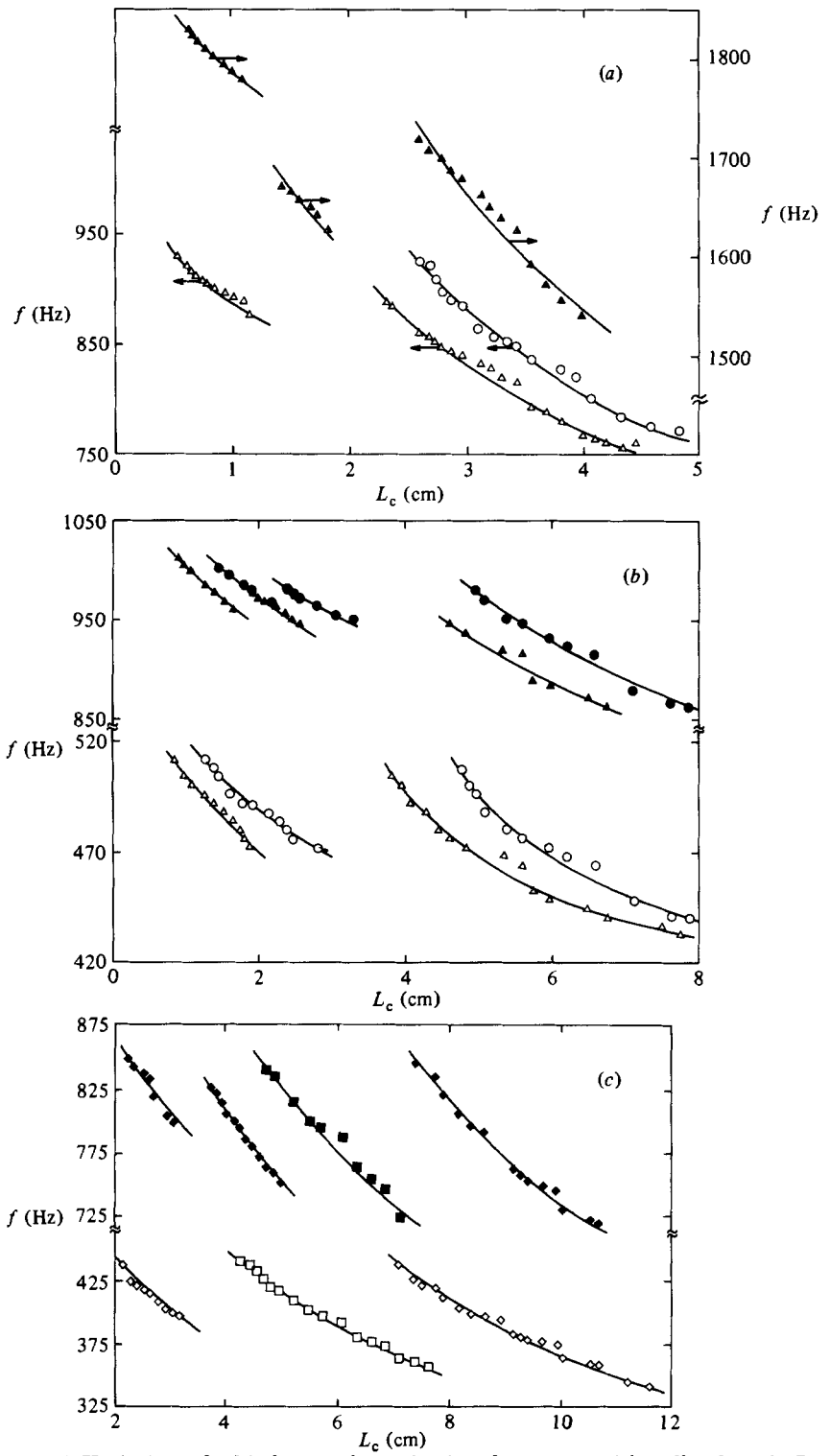

FIGURE 5. (*a*) Variation of whistler-nozzle excitation frequency with collar length L_c (cm) for halfwave mode (open symbols) and fullwave mode (solid symbols); $L_p = 15.24$ cm, $D = 2.54$ cm and $U_e = 36$ m s^{-1}: △, $h = 0.3175$ cm; ○, $h = 0.635$ cm. (*b*) f *vs.* L_c data for $L_p = 30.48$ cm, $D = 2.54$ cm, and $U_e = 36$ m s^{-1}; legend and symbol as in (*a*). (*c*) f *vs.* L_c data for $L_p = 30.48$ cm, $D = 7.62$ cm, $h = 0.635$ cm: □, $U_e = 36$ m s^{-1}; ◇, $U_e = 60$ m s^{-1}; legend as in (*a*).

layer. Consider figures 5*a* and 6*a* for $h = 0.3175$ cm first. Two modes one halfwave centred at $f \approx 900$ Hz and one fullwave centred at $f \approx 1800$ Hz, are excited simultaneously for $L_c > L_{c\,min}$. With increasing L_c, f decreases. Note that the halfwave mode is considerably stronger (by about 25 dB) than the fullwave mode and occurs for a larger range of L_c. The second stage appears for $L_c > 2.2$ cm and lasts for a much longer L_c range than the first stage. Note that the amplitudes near the peak in both stages are nearly equal. Both the halfwave and fullwave mode frequencies in the second stage are lower than those in the first stage. This is to be expected because L_c adds an effective length to L_p; the effective length is larger for the second stage than for the first stage. Based on our experimental data, the following relationship was obtained (Hasan & Hussain 1979) to predict the whistler frequency f:

$$\frac{f}{a_0 n}\left(L_p + C_1 \frac{L_c}{j} + C_2 D\right) = 1, \tag{1}$$

where a_0 is the acoustic speed, n ($= \frac{1}{2}, 1, \frac{3}{2}, \ldots$) denotes the mode and j ($= 1, 2, 3, \ldots$) the stage; our data showed that $C_1 = 1.65$ and $C_2 = 0.7$. Equation (1) is essentially the organ-pipe equation with end corrections. The curve representing (1) is not shown in figure 5 for clarity. When external excitation was applied in the absence of the flow, it was not possible to differentiate between the pipe resonance and the settling-chamber resonance.

For the larger h ($= 0.635$ cm), there is no dominant first stage, nor any fullwave mode in the second stage (figure 5*a*). Some humps in the $\tilde{u}$-spectra were detected for values of L_c corresponding to the first stage, but they were discarded on the basis of the amplitude criterion mentioned earlier. In this region, the $\tilde{u}$-signal trace did not show any change from the unexcited situation, nor was there any audible tone. For $h = 0.3175$ cm in the range $1.3\text{ cm} < L_c < 2$ cm, one single spectral peak at approximately the fullwave mode frequency occurs. This intermediate stage, which does not follow the patterns in stages I and II, has a frequency about 10 % lower than expected. The variation of u' along the length of the pipe nozzle for this intermediate stage suggested a very weak fullwave mode. Note that, with increasing L_c for any mode or stage, the increase in amplitude at the beginning of a stage is more abrupt than the decrease at the end of the stage (figure 6).

In each of the stages, f decreases with a progressive increase of L_c, as to be expected from the characteristics of the shear-layer tone (HZ) or other self-sustained oscillation phenomena. This suggests that the same basic mechanism which is responsible for the shear-layer tone or the jet tone triggers and sustains the whistler-nozzle oscillation.

Figures 5*b* and 6*b* show data for the $D = 2.54$ cm pipe nozzle of $L_p = 30.48$ cm. For both $h = 0.3175$ and 0.635 cm, there are two distinct stages of the halfwave mode accompanied by a weaker fullwave mode (figure 5*b*). Between stages I and II, there is a fullwave mode which corresponds to a shear-layer tone stage but not a whistler-nozzle stage. The amplitudes in these shear-layer tone stages are much lower (15–30 dB) than the amplitudes representing a whistler stage (figure 6*b*). Note that in figure 6*b* data for only $h = 0.3175$ cm have been presented.

(b) Turbulent initial condition

Figures 5*c* and 6*c* show the frequency and amplitude as functions of L_c for $D = 7.62$ cm at $U_e = 36$ m s^{-1} and 60 m s^{-1} with a fully developed turbulent boundary layer at the exit at either speed. In figure 6*c*, consider the $U_e = 60$ m s^{-1} case first. There are two stages of excitation: one is centred at $L_c \approx 2.6$ cm and the

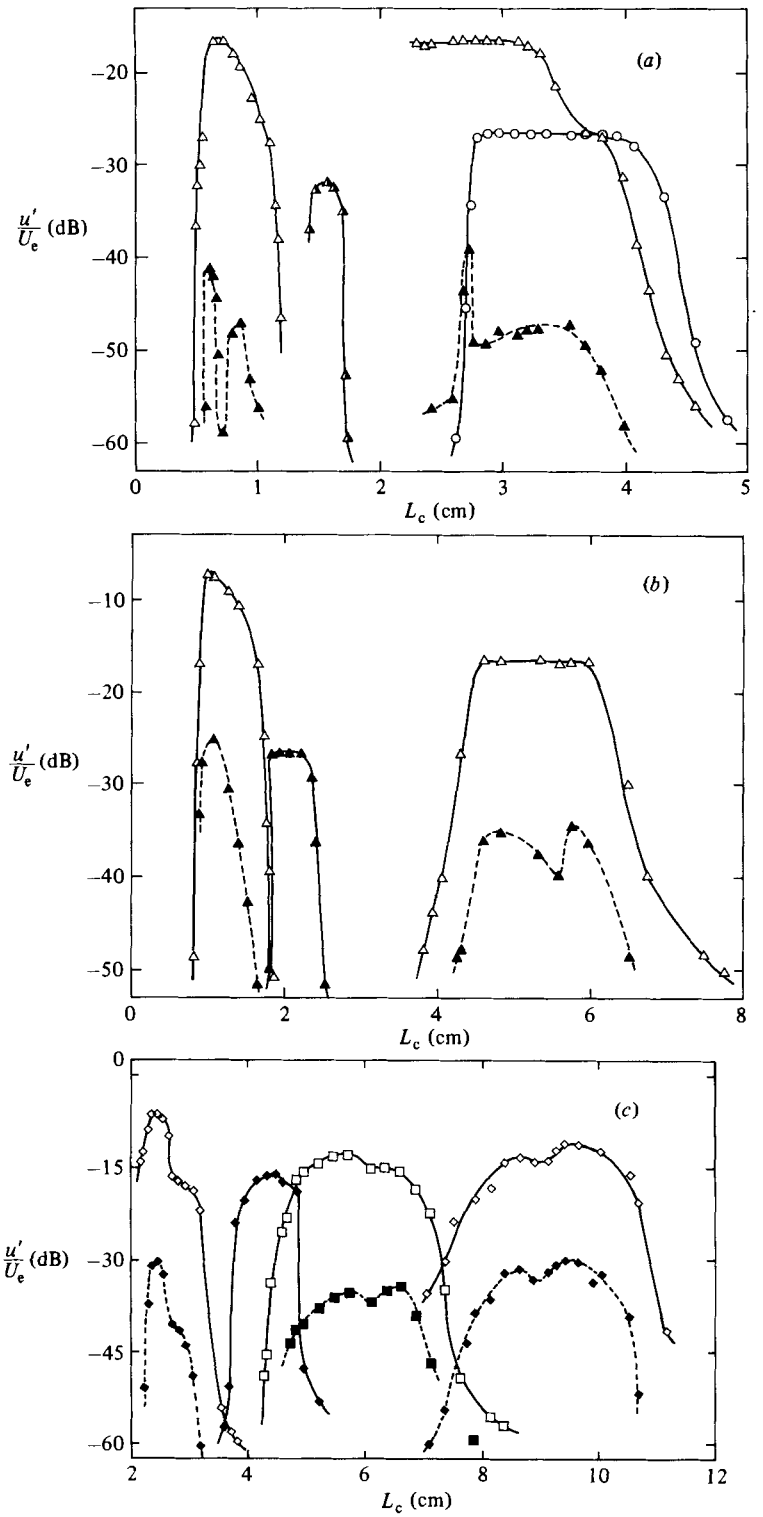

FIGURE 6. (*a*) Variation of amplitude at the pipe exit corresponding to the data in figure 5(*a*). (*b*) Variation of amplitude at the pipe exit corresponding to the data in figure 5(*b*). (*c*) Variation of amplitude at the pipe exit corresponding to data in figure 5(*c*).

other at $L_c \approx 9$ cm. Each of these stages is associated with both a halfwave mode and a fullwave mode. Note that, for either the fullwave or the halfwave mode, the frequencies in the two stages are nearly equal, the midfrequency being slightly lower in the second stage than in the first stage (figure 5*c*). This is analogous to the shear-layer tone phenomenon (see HZ).The second fullwave mode at $U_e = 60$ m s^{-1} (centred at $L_c \approx 4.5$ cm) is a shear-layer tone stage ($St_\theta \sim 0.01$) which is not supported by the pipe resonance and thus is not associated with a halfwave mode. At $U_e = 36$ m s^{-1}, there is only one stage of whistler excitation, consisting of simultaneous halfwave and fullwave modes. Note that (for $U_e = 60$ m s^{-1}) there is no whistler excitation in the range 5 cm $< L_c <$ 7 cm.

The shear-layer tone-type behaviour of the whistler nozzle suggests that the shear layer from the pipe lip rolls up into discrete vortical structures. Detailed profile data show that the pipe-exit boundary layer is fully turbulent for either value of U_e when $D = 7.62$ cm. Thus, in these cases, the initially fully turbulent shear layer also rolls up into vortical structures. (The roll-up and organization of initially full turbulent shear layers into discrete vortical structures was first demonstrated by Clark & Hussain (1979) via visualization and ciné films. Recently, the roll-up of an initially fully turbulent plane mixing layer has been demonstrated and the resulting coherent structure details have been educed by Hussain & Zaman (1982).) This shear-layer tone for a turbulent boundary layer, though much weaker than that for an initially laminar shear layer, is accentuated by the pipe-nozzle resonance if one of its organ-pipe modes matches the shear-layer tone frequency.

In view of the fact that the roll-up of the initially turbulent shear layer into discrete coherent structures will have large dispersion in formation distance, strength, etc., the start of the whistler excitation tone is likely to be less abrupt when the layer is initially turbulent than when initially laminar. Data in figure 6(*c*), when compared with those in figures 6(*a*, *b*), show consistency with this notion. Furthermore, the vortices in the initially turbulent cases are likely to induce weaker feedback and consequently weaker whistler excitation, not only because of diffuse vorticity but also because of phase and amplitude jitter from one structure to another. As figure 6*c* shows, the peak amplitudes are weaker than in the cases when the shear layer is initially laminar; this was found to be always true. For $U_e = 36$ m s^{-1}, the turbulent case amplitude is 10 dB lower than that in the laminar case. Note that the rise in amplitude with increasing L_c is sharper for shorter L_c, because at shorter L_c the rolled-up vortices are stronger (owing to higher coherent vorticity) and thus capable of producing stronger feedback.

From the data of figure 5 it can be summarized that the frequency behaviour of the whistler nozzle is similar to the shear-layer tone (f decreases with increasing L_c). But the range over which the frequency changes in any stage is very limited, since the requirement for shear-layer tone and organ-pipe resonance must be satisfied simultaneously. It is found that the shear-layer tone frequency is always a multiple of the fundamental frequency having an St_D value in the range (0.3–0.6) of the 'preferred mode' of the jet (Hussain & Zaman 1981).

(*c*) *Interstage gaps*

A difference between the whistler nozzle and the shear-layer tone excitations can be identified from figures 5(*a–c*). In the shear-layer tone phenomenon, there is always an excitation frequency for every value of the lip–wedge distance within its range of operation; one stage always gives way to the next, typically with an overlap range. Since the whistler phenomenon is the coupling of two resonance mechanisms,

excitation will occur when the conditions for both resonances are satisfied simultaneously. Clearly, there will be ranges of L_c where conditions for both resonances cannot be satisfied. Because of this, there are interstage ranges of L_c where whistler-nozzle excitation does not occur (see figures 5*a–c*). However, in these 'dead zones', the shear-layer tone should still occur in the region between the collar and pipe lips. However, compared with the tone induced by a sharp wedge (see HZ), the shear-layer tone will also be considerably weaker.

3.3. *Excitation amplitude at pipe exit*

The amplitude of whistler excitation depends on U_e, L_p, L_c and h. For a given L_p, h and U_e, the amplitude can be controlled primarily by changing the collar length L_c. Figure 7 gives one typical example of the variation of excitation amplitude u'_e/U_e (at the pipe-exit centreline) as a function of L_c; I and II denote the first and second stages. The sensitivity of the amplitude to the step height h is also included in figure 7. Note that, when h is increased, the collar length must also increase in order for the shear layer to impinge on the collar lip. The vortices get correspondingly more diffuse and the tone amplitude is weaker and its rise is less abrupt. Note that, in order to produce a given amplitude of excitation, it is preferable to choose an L_c corresponding to the right-hand side of a stage because the change in amplitude is more gradual and less sensitive than on the left-hand side. Figure 7 shows that the whistler nozzle can be used to introduce controlled excitation of selectable amplitudes by appropriately choosing L_c. It has been shown that the response of the jet to controlled self-excitation (see HH) is similar to that of imposed excitations (Zaman & Hussain 1980; Kibens 1980).

3.4. *The shear-layer characteristics for the whistler-nozzle excitation*

The evolution of whistler-tone amplitude and phase profiles are shown in figure 8 for the first-stage excitation, for $L_p = 30.48$ cm, $D = 2.54$ cm, $L_c = 1.02$ cm and $u'_e/U_e = 12\,\%$. The measurements were made at three different x-stations: two inside the collar ($x = 0.254$ and $x = 0.635$ cm) and one outside ($x = 2.54$ cm). The whistler fundamental tone phase and amplitude profiles are given in figures 8 (*a*, *b*) respectively. Because of the backflow problem, the momentum thickness θ_1, for the data in figures 8(*a*, *b*), was calculated as follows:

$$\theta_1 = \int_{y_{0.95}}^{y_{0.25}} \frac{U}{U_c}\left(1 - \frac{U}{U_c}\right) \mathrm{d}y.$$

That is, the integration was terminated at the y-location where the mean velocity was $0.25U_c$.

Inside the collar, the perturbation phase remains constant for $(y - y_{0.5})/\theta_1 \lesssim -1$ (figure 8*a*), then increases to a peak and suddenly drops by about π near $(y - y_{0.5})/\theta_1 \approx 2$. These profiles are in qualitative agreement with the shear-layer tone data (HZ). At each value of x, the radial location of the maximum phase gradient $(\mathrm{d}\phi/\mathrm{d}y)_{\max}$ coincides with the minimum of the tone amplitude u'_f (figure 8*b*), consistent with the prediction of linear spatial stability theory (Michalke 1965). Note that the locations of the u'_f peak and the minimum move towards the jet centre with increasing x. In the shear-layer tone, the transverse location of the u'_f minimum was the same at different x.

For the convenience of comparison of whistler-nozzle data with other experimental and theoretical data, the u'_f data for $x = 0.254$ cm are plotted in figure 8*c* in a different non-dimensional transverse coordinate. Also included in figure 8*c* are Michalke's

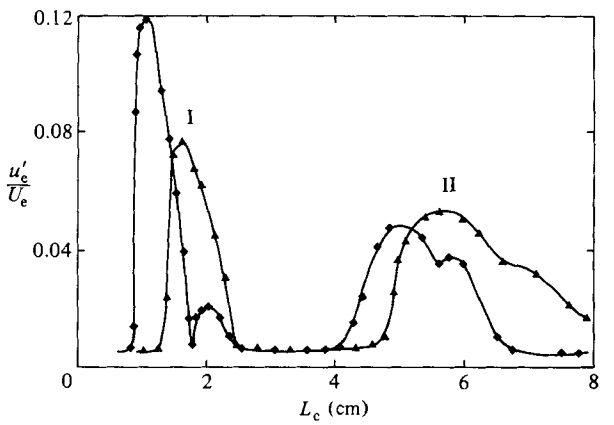

FIGURE 7. Variation of pipe-exit fluctuation intensity u'_e/U_e with L_c for $L_p = 30.48$ cm, $U_e = 36$ m s^{-1} and $D = 2.54$ cm: ◆, $h = 0.3175$ cm, ▲, $h = 0.635$ cm.

inviscid theory (for laminar flow) and Rockwell's (private communication) data for organized wave in an impinging turbulent jet. Each curve in figure 8*c* is identified with two Strouhal numbers, except for Michalke's theoretical prediction. The first Strouhal number $St_{\theta e}$ is based on the exit momentum thickness and the second one is based on the local momentum thickness θ. Note that in the present case θ was calculated as

$$\theta = \int_{y_{0.95}}^{y_{0.125}} \frac{U}{U_c}\left(1 - \frac{U}{U_c}\right) dy,$$

thus partly accounting for the St_θ values being lower than those in the cited references.

Two different cases of Rockwell's data are included. The first case represents the organized wave data for the oscillation dominated by the instability wave ($St_\theta = 0.025$), and the second case represents the data where instability and acoustic waves have nearly equal amplitudes at separation ($St_\theta = 0.041$). These two cases are included in order to permit comparison between similar situations. The general agreement of the whistler data with Michalke's theory suggests that the inviscid parallel-flow stability theory may be adequate to describe the overall character of the whistler-tone amplitude distribution in the axisymmetric mixing layer. On the high-speed side away from the shear layer, the fundamental amplitude in the whistler tone is higher because of the surging of the core flow. The similarity between these and Rockwell's data also suggests that a similar mechanism is at work here.

3.5. *Streamwise phase variation and wavelength*

The streamwise phase variation of the disturbance wave is necessary to deduce its phase velocity and wavelength, to understand the superposition of vorticity (i.e. hydrodynamic) and acoustic waves, and to see if the phase difference between the separation ($x = 0$) and impingement ($x = L_c$) points are consistent with the 'phase criterion'. In the case of self-sustained oscillations, this criterion requires that the feedback from the impingement point should reach the separation point at the appropriate phase in order to reinforce and sustain the underlying instability phenomenon crucial for the flow self-excitation (see HZ).

It is clear that, in order for a purely hydrodynamic wave to become resonant, an integral number of wavelengths must fit into the separation–impingement length, viz L_c in the present case. This simply indicates that the net phase difference ϕ_{si} between

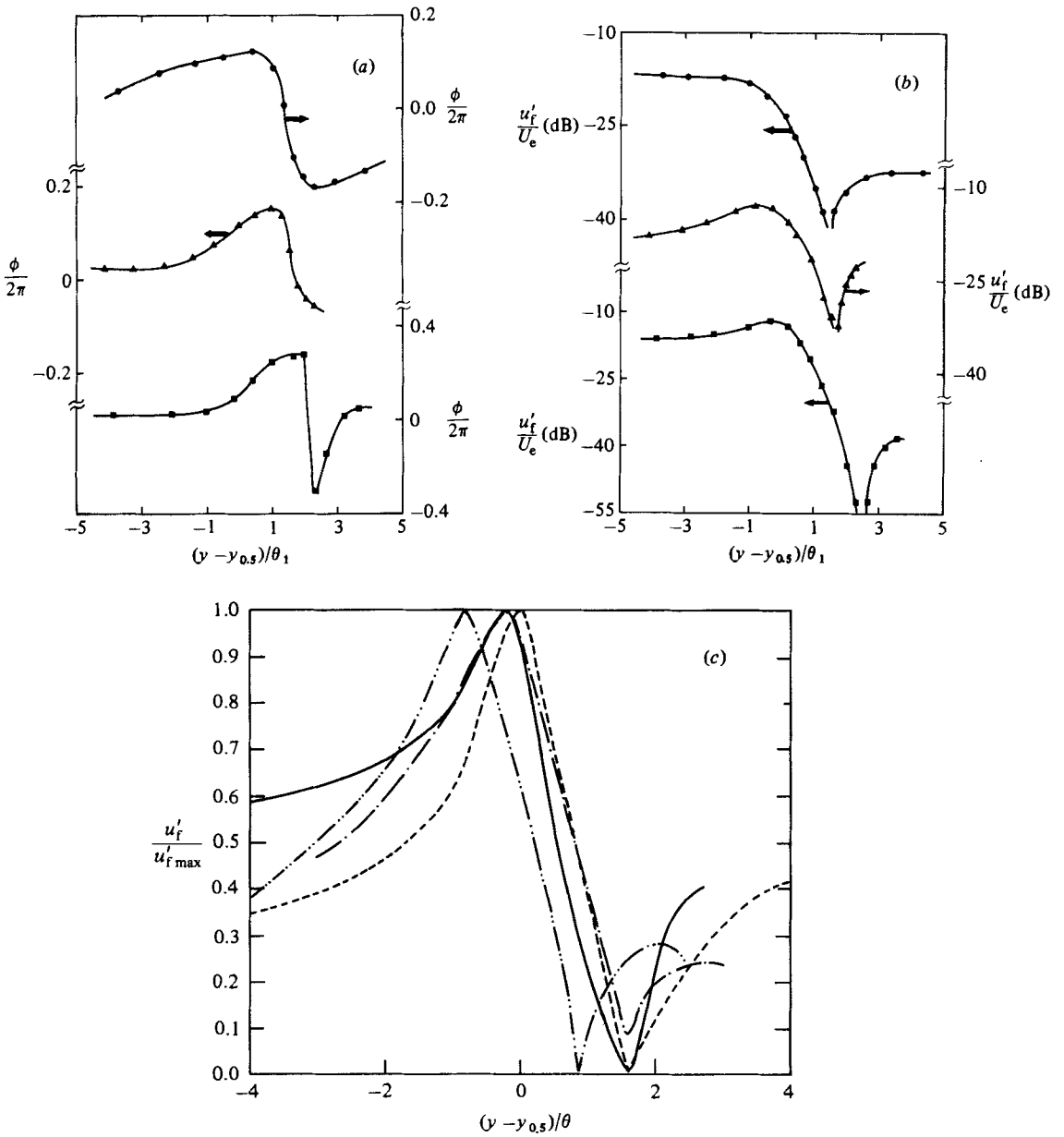

FIGURE 8. (*a*) Phase profile across the shear layer for $D = 2.54$ cm, $L_p = 30.48$ cm, $f = 504$ Hz, $U_e = 36$ m s^{-1}: ■, $x = 0.254$ cm; ▲, 0.635 cm; ●, 2.54 cm. (*b*) Profile of u'_f across the shear layer corresponding to the data in (*a*). (*c*) Amplitude profiles for disturbance tone: ——, whistler (0.006, 0.0135); – – – – – –, Michalke's theory (0.017); —·—·—, Rockwell (0.017, 0.025); —··—··—, Rockwell (0.0275, 0.041).

separation and impingement points must be $2n\pi$, where n is the number of wavelengths between $x/L_c = 0$ and $x/L_c = 1$. However, earlier theoretical models as well as experimental data indicate that $\phi_{si} = 2\pi(n+A)$, where A is an empirical constant representing an additional distance as a fraction of a wavelength. This reduces the phase criterion to $L_c/\lambda = n+A$ (see later).

In the case of jet-edge tone, Brown (1937) deduced from his smoke pictures that $A \approx \frac{1}{4}$. Curle (1953) and Powell (1961) also used the same value (i.e. $A = \frac{1}{4}$) in their

theoretical models of the slit-jet edgetone. For shear-layer tone, HZ found $A \approx \frac{1}{2}$, a value also found by Sarohia (1977) for self-excitation of a shear layer over a resonant cavity. Crighton & Innes (1981) predicted a value of $A = \frac{7}{8}$ for the shear-layer tone. On the other hand, the value of A was found to be zero in the self-excited flow studies by RS, Knisely & Rockwell (1981) and Ho & Nosseir (1981). Perhaps the value $A = 1$ found by Ziada & Rockwell (1982) can be dismissed as an error in their identification of stages, so that their study also suggests $A = 0$.

A number of factors can contribute to non-zero values of A: viz. shear layer characteristics at impingement, flow geometry, disturbance phase profile and phase distortions. The phase criterion of $A = 0$ will be consistent only for an infinitesimally thin pendulating shear layer. The gradual spreading of the shear layer due to viscous diffusion requires consideration of the non-parallel effect. Furthermore, the assumption that the feedback is most stable at the instant when the vortex centre is at the wedge tip is true only if the vortex is irrotational; the finite radius of a viscous vortex must make $A > 0$. Also, the wavelength will vary in x due to non-parallel and nonlinear effects. If the shear layer is turbulent before impingement, the vortex size will be still larger, producing a larger value of A.

The transverse displacement of the impingement edge also should contribute to A being non-zero. The disturbance phase is not constant across the shear layer. While, in a thin (inviscid) layer, there will be a 180° abrupt phase jump, the phase variation will be smoother in a viscous shear layer. The presence of a strong acoustic disturbance can further distort the phase profile (see RS).

The geometrical considerations perhaps require that values of A should be compared only for similar geometries. Thus, while the slit-jet tone should have $A > 0$, the conflicting values of A found in different investigations in shear layers need explanation. Of the factors considered above, the key factor is the phase profile. The transverse phase gradient in the shear-layer tone at any x led HZ to recognize the importance of the transverse location for streamwise phase measurement. HZ measured $\mathrm{d}\phi/\mathrm{d}x$ at the transverse location of maximum phase lead. RS found a 'phase core' in an axisymmetric impinging cavity flow and found $A = 0$ from measurement in this core, for an instability-wave-dominated excitation case. In the present situation where a strong acoustic wave is simultaneously present with the instability wave, the difference between $\phi(x)$ data along the centreline and along the $U/U_c = 0.95$ line clearly suggests that the 'phase-core' region is small.

In general, we recommend the high-speed edge of the mixing layer, namely, the $U/U_c = 0.95$ line, for $\phi(x)$ measurement, independent of whether a 'phase core' exists or not. Since the phase measurement is sensitive to the disturbance amplitude, $\phi(x)$ should ideally be measured at the location of maximum disturbance amplitude (see HZ). On the other hand, in order to avoid the ambiguity of $\phi(x)$ data near regions of steep gradient in $\phi(y)$, the measurement should be made away from the middle of the shear layer. Also, if the shear layer is turbulent, meaningful $\phi(x)$ data can be taken only at the edge of the shear layer. Hence, the $U/U_c = 0.95$ line is the optimum choice. It may be important to note that HZ found the phase profiles $\phi(y)$ nonsimilar at different x.

The above discussion thus suggests that variations in A are to be expected between different experiments. Further investigations are necessary to relate definitively variations in A with various controlling factors.

The streamwise variation of the phase of the $u(t)$ signal along the centreline and along the high-speed edge, viz along the line corresponding to $U/U_c = 0.95$, are shown in figure 9 for a variety of whistler-nozzle excitation situations. All the data

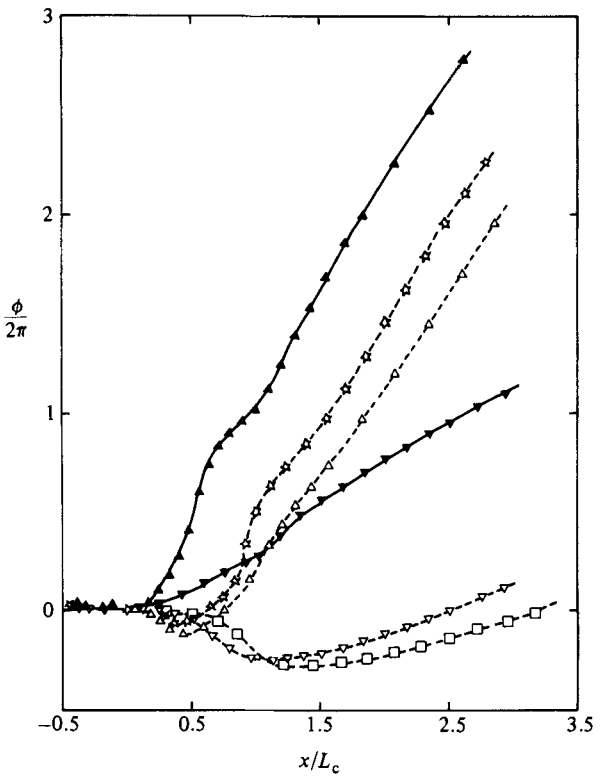

FIGURE 9. Streamwise phase variation for $D = 7.62$ cm, $L_p = 30.48$ cm along the centreline (open symbols) and along $U/U_c = 0.95$ line (solid symbols). The frequency (Hz), stage and velocity (m s^{-1}) are □, 420, I, 45; ▽, 394, I, 60; △, 372, II, 60; ☆, 366, II, 45.

correspond to the fixed excitation amplitude $u'_e/U_e = 2\%$. Note that the phase distributions along the centreline (open symbols) and the $U/U_c = 0.95$ line (solid symbols) are not identical. In this figure, the pipe exit and collar exit are located at $x/L_c = 0$ and $x/L_c = 1$ respectively. The phase remains virtually constant inside the pipe (i.e. $x/L_c < 0$), indicating the dominance of the acoustic wave there. Note the high streamwise phase gradients between $x/L_c = 0$ and $x/L_c = 1$, after which the phase distributions become nearly linear with x. Similar phase gradients were predicted by RS's one-dimensional model for an impinging axisymmetric cavity flow, where the instability and acoustic waves were comparably dominant. Note that, in figure 9, the phase difference between stages I and II at the impingement point ranges between π and 1.57π; for a purely hydrodynamic oscillation, this value should be 2π.

3.6. *Phase velocity and h/λ relations*

Let us represent the disturbance wave as

$$\begin{aligned}\tilde{u} &= \tfrac{1}{2}\hat{u}(y)\,\mathrm{e}^{\mathrm{i}(\alpha x-\omega t)} + \text{conjugate}\\ &= \tfrac{1}{2}\hat{u}(y)\,\mathrm{e}^{\mathrm{i}\alpha(x-ct)} + \text{conjugate},\end{aligned} \tag{2}$$

where $\alpha = \alpha_i + \mathrm{i}\alpha_r$ and $c = c_i + \mathrm{i}c_r$ and $\omega = \alpha c$ is the circular frequency. The phase velocity v_{ph} is then given by $v_{ph} = \omega/\alpha_r$. Assuming nearly parallel flow, if ϕ denotes the phase of $\tilde{u}$, it is clear that $\alpha_r = \mathrm{d}\phi/\mathrm{d}x \equiv 2\pi/\lambda$. Thus, from the streamwise phase gradient, both the wavelength and the phase velocity v_{ph} can be inferred. The phase velocities calculated from the phase distributions of figure 9 are shown in figure 10.

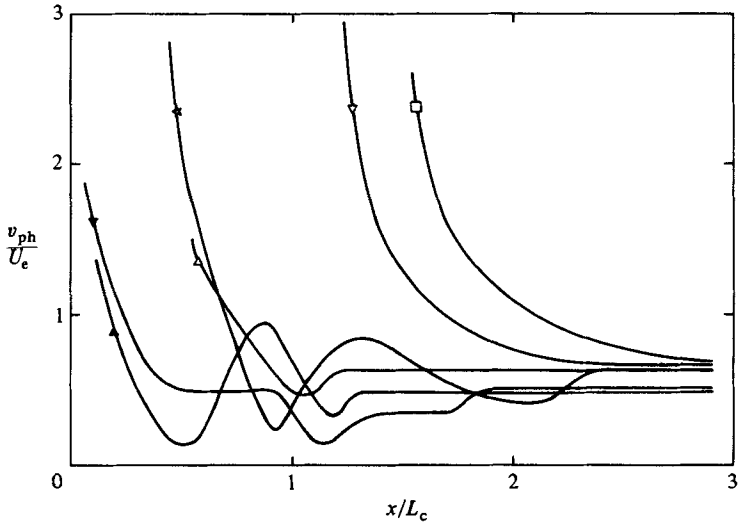

FIGURE 10. Streamwise variation of v_{ph}. For symbols see figure 9.

U_e (m s^{-1})	f (Hz)	(Stage)	$\frac{v_{ph}}{U_e}$	$\frac{L_c}{\lambda}$
60	434	(I)	0.805	0.1827
	374	(II)	0.675	0.891
	416	(I)	0.761	0.22
	372	(II)	0.678	0.894
45	392	(II)	0.621	0.945
	366	(II)	0.628	1.06
	244	(I)	0.738	0.1866
30	392	(II)	0.755	0.924
	242	(I)	0.907	0.185
	240	(II)	0.619	0.895

TABLE 2. v_{ph} and L_c/λ data for $D = 7.62$ cm

Note that the phase velocity v_{ph}, which equals the acoustic speed within the pipe, decreases rapidly with increasing x and approaches an asymptotic value outside the collar. The rapid drop of the phase velocity with x in figure 10 should give an idea of the location from where onwards the hydrodynamic wave dominates the acoustic wave. Note that the phase velocity v_{ph} reaches constant values around $0.6U_e$ with increasing x. These values are in general agreement with the data of Ko & Davies (1971), Lau, Fisher & Fuchs (1972), Bradshaw, Ferris & Johnson (1964), Petersen (1978) and Hussain & Clark (1981).

In order to estimate the relationship between L_c and λ, the value of λ within the collar would be more meaningful. However, because of the large variation of the phase velocity within the collar, it is not possible to have an accurate estimate of λ within the collar. So, an estimate of the wavelength λ in the region ($x/L_c > 2$) where v_{ph} becomes nearly constant was made. Based on this λ, the L_c/λ values for different velocities and stages are listed in table 2; these values do not appear to support a simple relationship of the type $L_c/\lambda = n + A$, expected for self-sustained oscillation phenomena. However, if λ is inferred from the distribution of tone amplitude within the collar (see figure 4*b*), a relationship of the type $L_c/\lambda = n + A$ appears reasonable.

3.7. *Flow visualization*

In an effort to demonstrate that the whistler-nozzle excitation is triggered when vortices in the shear layer within the collar interact with the collar lip, flow visualization was carried out by introducing $TiCl_4$ smoke upstream of the pipe nozzle. When the excitation is present, one would expect to see a vortex at the collar exit especially when the pipe exit flow is laminar. The visualization was done for $L_p = 30.48$ cm ($D = 2.54$ cm) at $U_e = 16$ m s^{-1}. Natural roll-up of vortices in the unexcited jet takes place at $x/D \approx 2$ (figure 11*a*). Figure 11*b* shows the condition when whistler excitation is present. For both excited and unexcited conditions, the pipe exit location is shown by an arrow. Flow visualization showed that the shear layer rolls up sooner in x owing to the feedback effect during whistler excitation, as should be evident from comparison of figures 11*a* and *b*. Similar efforts to visualize the flow with turbulent initial conditions failed to reveal any clear vortex structure. It was not considered worthwhile to visualize the flow within the collar by redesigning the facility with transparent pipes and collars.

3.8. *Non-dimensional representation of the whistler-nozzle phenomenon*

Non-dimensional relationships between the controlling parameters would be helpful in optimum choice of whistler-nozzle dimensions and prediction of its performance in various technological applications. Included among the controlling parameters are L_p, L_c, D, U_e and h. Clearly, L_p and L_c are dominant parameters. Since L_c depends on h, it may not be necessary to include h directly. If the whistler excitation is triggered by a shear-layer tone, which in turn must depend on the instability of the shear layer (HZ) downstream of the pipe nozzle, then the phenomenon must depend on the state of the boundary layer at the pipe exit. A lengthscale of the boundary layer, say the momentum thickness θ_e, must therefore be included. Based on our experiments with the shear-layer tone (HZ), it would appear that non-dimensional frequencies $St_c (= fL_c/U_e)$ and $St_{\theta e} (= f\theta_e/U_e)$ would be important characteristic parameters of the whistler nozzle. When St_c *vs.* L_c was plotted, data did not collapse for different L_p values. However, when the St_c data were plotted against L_c/θ_e, the data collapsed for both $L_p = 30.48$ cm and $L_p = 15.24$ cm (figure 12*a*); St_c values based on the fullwave mode frequency are also shown in figure 12(*a*). Note that the collapse of the data is comparatively better for the halfwave mode than for the fullwave mode. This collapse suggests that the initial momentum thickness θ_e is an important parameter for the whistler phenomenon and emphasizes the role of the shear-layer tone in the phenomenon.

The variation of St_c with L_c/θ_e is nearly linear; data for different stages fall essentially on the same line. This is not so for the shear-layer tone, the jet tone or other self-sustained oscillations. For the shear-layer tone (HZ) and the cavity flow (Sarohia 1977), St_c varies almost linearly in each stage, but different stages are separated by vertical shifts. In figure 12*a*, the first and second stages are not separated and appear to fall on a single line. The nearly linear variation of St_c indicates that, even though the shear-layer tone triggers the phenomenon, it is primarily an organ-pipe resonance.

Equation (1) can be used to interpret the results in figure 12. If C_1/j is neglected (i.e. because $C_1/j \ll L_p/L_c$), and considering the fact that $C_2 D \ll L_p$, (1) can be approximated as

$$St_c = \frac{n}{M}\frac{L_c}{L_p}, \tag{3}$$

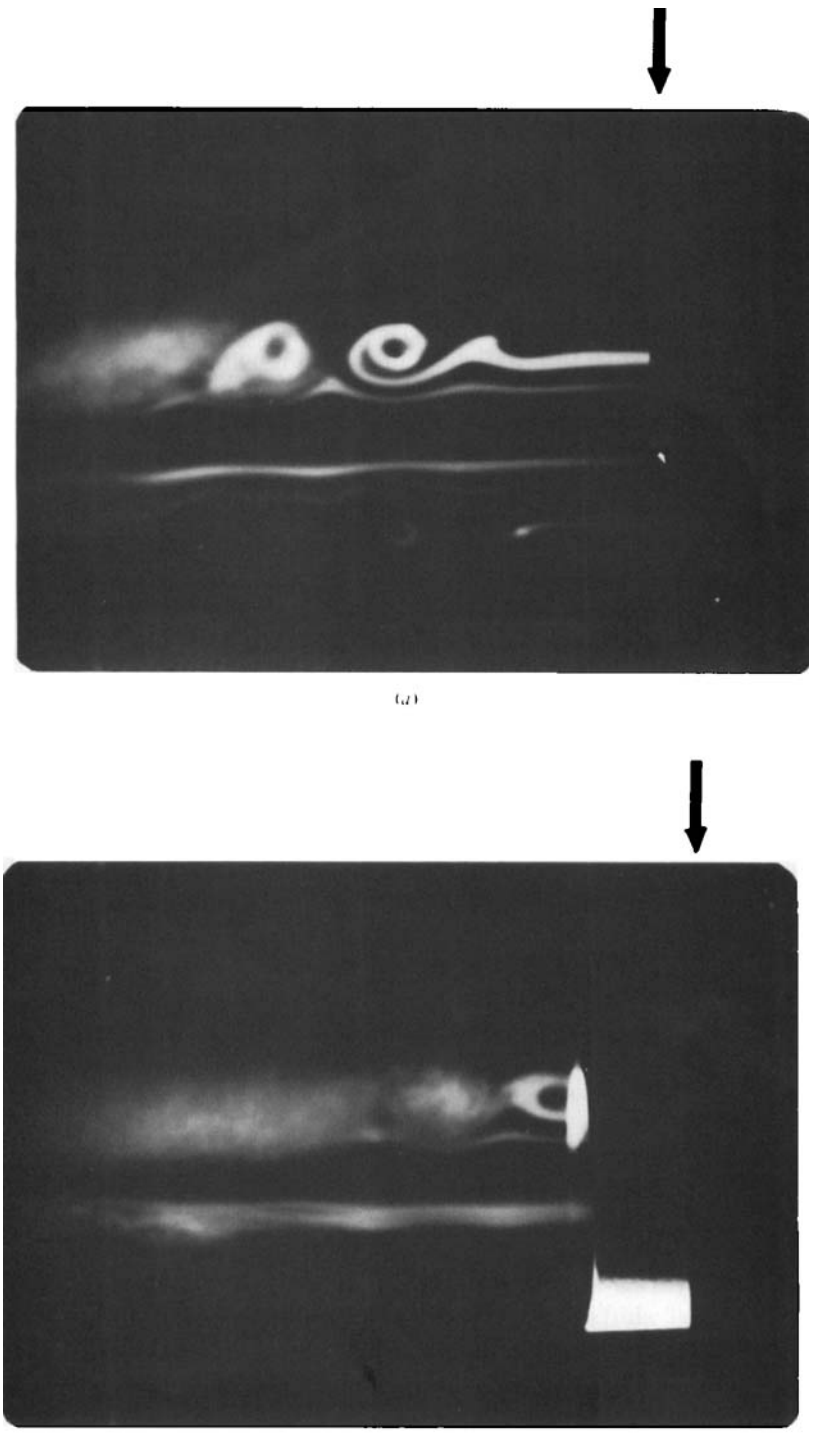

FIGURE 11. Flow visualization for $L_p = 30.48$ cm, $D = 2.54$ cm at $U_e = 16$ m s^{-1}; (*a*) unexcited ($L_c = 0$); (*b*) excited ($L_c \neq 0$). The arrow indicates the location of the pipe exit. Flow is from right to left.

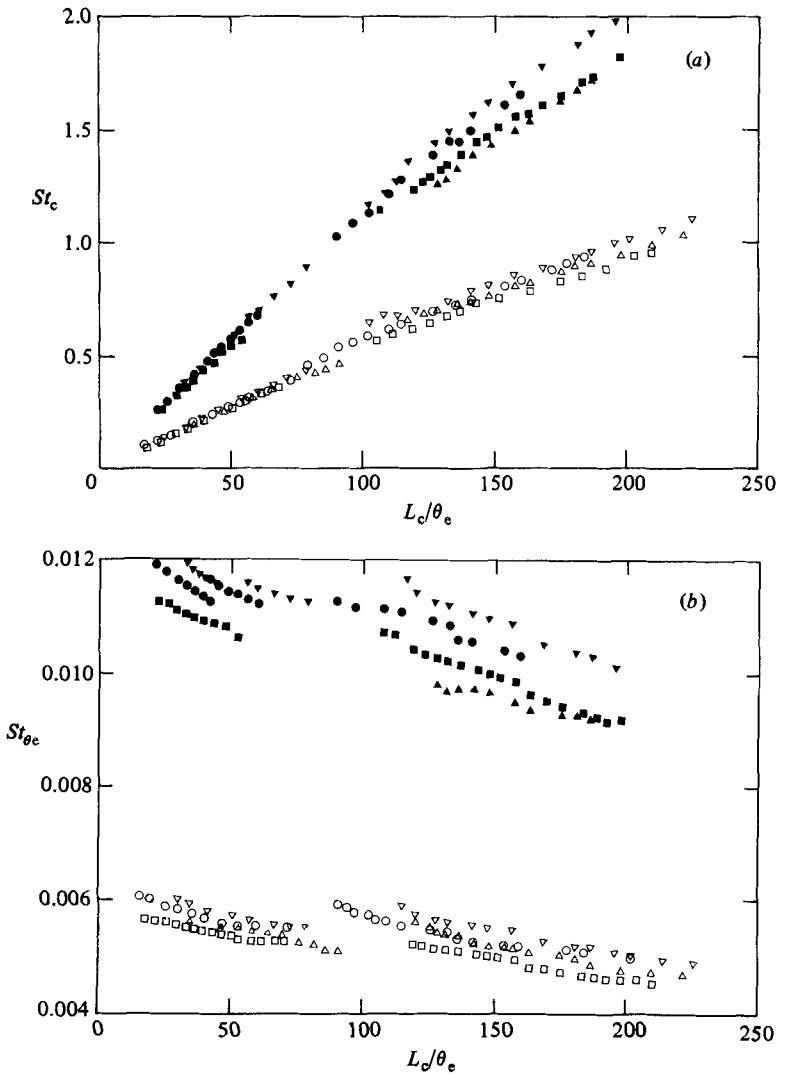

FIGURE 12. (*a*) Variation of St_c with L_c/θ_e; L_p (cm) and step height (cm) are □, 15.24, 0.3175; △, 15.24, 0.635; ○, 30.48, 0.3175; ▽, 30.48, 0.635. Open symbols denote halfwave mode and solid symbols denote fullwave model. (*b*) Variation of $St_{\theta e}$ with L_c/θ_e; symbols as in (*a*).

where M is the Mach number. Note that (3) predicts a linear variation of St_c with L_c. Note that the collapse of St_c data in figure 12(*a*) is much better in the first stage than in the second because the assumption $C_1/j \ll L_p/L_c$ is more appropriate in the first. From (3) one can conclude that the $St_{\theta e}$ *vs.* L_c/θ_e data for different velocities and modes of resonance will not collapse.

Figure 12(*b*) shows the data of figure 12(*a*), plotted as $St_{\theta e}$ $(= f\theta_e/U_e)$ *vs.* L_c/θ_e. If St_c *vs.* L_c/θ_e were exactly linear, then $St_{\theta e}$ would be a constant. Data in figure 12(*b*) show that in each stage $St_{\theta e}$ decreases with increasing L_c – a characteristic of the shear-layer tone (HZ). However, unlike the shear-layer tone, the decrease in $St_{\theta e}$ with increasing L_c/θ_e is quite gradual, decreasing from about 0.006 to about 0.0045 over the range $0 < L_c/\theta_e < 250$. The gradual fall-off of the St_c values from linear variation with increasing L_c in figure 12(*a*) and the corresponding decreasing values of $St_{\theta e}$ in figure 12(*b*) are to be expected, because increasing values of L_c produce longer

effective lengths of the pipe nozzle and hence lower excitation frequencies. Because the phenomenon consists of two independent resonance mechanisms, and there are controlling parameters not included in $St_{\theta e}$, it is not expected that $St_{\theta e}$ data will collapse. Even so, it is quite impressive that data for different controlling parameters fall in a narrow band. Note that the tendency for the shear-layer tone stages to fall into separate curves (see HZ) is smoothed by the organ-pipe resonance. The collapse of the data, when non-dimensionalized by θ_e, emphasizes the important role of the shear-layer tone phenomenon in whistler-nozzle excitation.

3.9. *Whistler excitation in pipe–ring and pipe–hole configurations*

Our explanation for the whistler-nozzle phenomenon was subjected to further scrutiny in ring- and hole-tone configurations. Even though the above data adequately characterize the whistler-nozzle behaviour as a function of the values of the controlling parameters, these data and their discussions in the foregoing establish well that while the device configuration, as well as the control of the excitation amplitude and frequency, is extremely simple, the phenomenon is not. The data support our explanation rather well, even though some peculiarities in the details remain unexplained.

Two aspects of the whistler nozzle would negate total success of any simple explanation. Since the phenomenon is the confluence of two independent resonance mechanisms, it is not likely that a simple nondimensional relation can be valid for the entire range of its operation. Such a simple relationship does not necessarily include all controlling parameters; the less-dominant parameters would produce additional deviations from the modelled simple relationship. The second aspect complicating a simple explanation is, of course, the collar. Because of the unavoidable recirculating region (downstream from the pipe exit) within the collar, the whistler tone must produce periodic modulation of the recirculating flow and periodic ingestion of the ambient fluid. The collar, depending on its length, also alters somewhat the initial condition, i.e. the details of the boundary layer at the exit of the pipe nozzle. The additional complicating feature of the collar is that its lip does not constitute a sharp edge as is typical in shear-layer tone and jet tone phenomena. Studies with a sharper collar lip were discarded because of the additional complications of the cavity that had to be introduced within the collar in order to produce the sharp lip.

In order to substantiate further our explanation of the phenomenon discussed in the previous sections, it was considered necessary, even highly instructive, to carry out additional experiments with the whistler nozzle in the absence of the collar. If our explanation was correct, then it should be possible to induce the whistler nozzle excitation in the absence of the collar by placing either a ring or a hole at the location of the collar lip. In either of these configurations, respectively called pipe–ring and pipe–hole, the recirculating region (which is present for the collar excitation) is eliminated, and there is entrainment of the ambient fluid right from the origin of the mixing layer.

The whistler excitation with a ring and a hole was separately studied with a 2.54 cm diameter pipe nozzle of length (i.e. L_p) 15.24 cm. In each case, the traversing axis was carefully aligned with the pipe-nozzle axis. A precision cylinder which slides snugly into the nozzle as well as the ring or the hole, when in place, was used to check that the ring or the hole axis was aligned with the nozzle axis for all downstream traverses. Both the ring and the hole were so held that the impinging lip was far from

the support so that the support did not interfere with the phenomenon. The pipe nozzle, of thickness 0.3175 cm, was machined square at the downstream end, which thus forced the initial entrainment to be normal to the mainstream (figure 1 *d*) rather than essentially parallel (figure 1 *e*). Detailed data by Husain & Hussain (1979) showed that the two different initial entrainment patterns produce no difference in the time-average measures or instability details of the initial shear layer. In order to record the amplitude and frequency data, the hot wire was placed slightly downstream of the pipe nozzle (i.e. $x = 0.2$ cm) and near the high-speed edge of the mixing layer, i.e. $U/U_e = 0.95$. This location was chosen so that the sensor was away from the impingement point and yet captured the 'shear-layer tone' in the axisymmetric mixing layer. The ring or the hole will in general induce 'shear-layer tones' in the axisymmetric configuration; only when the shear-layer tone matches an organ-pipe mode of the pipe nozzle will a whistler tone be excited. Unless otherwise specified, 'shear tone' in this section will denote those induced by the ring or the hole but not supported by the pipe nozzle. The latter will be denoted as 'whistler tone'. The measurement probe was inserted through the ring or the hole (figures 1 *b*, *c*) so that probe-induced shear-layer tone (see HZ) was avoided. In general, the peak amplitudes of the whistler excitation with the ring or the hole were lower than those with the collar. The audible tone was also louder with the collar, indicating that the collar accentuates the sound via the increased radiating surface and enhanced flow surging.

The results of the whistler-excitation experiments in the modified configurations involving the ring and the hole are summarized in figures 13 and 14 for three different speeds: $U_e = 10$ m s^{-1}, 24 m s^{-1} and 36 m s^{-1}. Figure 13 (*a*) shows the frequency as a function of the downstream separation b of the hole or the ring from the pipe nozzle. Note that the frequencies fall in three ranges ($f \approx 450$ Hz, 1800 Hz, 2600 Hz) corresponding to the shear tone at the three speeds. However, the whistler-tone mode ($f \approx 900$ Hz) falls in a small range corresponding to the halfwave mode of the pipe nozzle. The non-dimensional frequency St_b ($= fb/U_e$) is shown in figure 13 (*b*). Figure 13 (*c*) shows the frequency data in terms of $St_{\theta e}$ ($= f\theta_e/U_e$), where θ_e is the exit momentum thickness of the boundary layer.

The data in figure 13 show two trends of the frequency variation with b. For a given U_e, as b is increased, the shear-tone frequency f_s should progressively decrease. However, the organ-pipe mode frequency f_p remaining unchanged for a given L_p, the nozzle would tend to limit the shear-tone frequency to an organ-pipe frequency. If f_s is significantly different from f_p, the variation of f_s with b will be monotonic. This is the case for $U_e = 10$ m s^{-1}. However, if f_s were close to f_p or its harmonics (which would correspond to higher modes like fullwave, one-and-a-halfwave, etc.), then the overall variation of the frequency would be like that of the shear tone. However there will be ranges of b over which the shear-tone frequency will 'lock in' with the organ-pipe tone. In figure 13 the 'steplike' frequency variations are clear; the constant frequency ranges indicate 'lock in'. In the non-dimensional coordinates shown in figure 13 (*c*), note that the three distinct shear tone stages in figure 13 (*a*) collapse. The corresponding $St_{\theta e}$ range is 0.01–0.014, agreeing closely with the shear-layer tone data of HZ. Note that there are a total of four shear-tone stages, the number of stages increasing with U_e. Note that the shear-tone stages in pipe–ring and pipe–hole configurations agree identically with the plane shear-layer-tone data of HZ, also shown in figure 13 (*b*). It is quite impressive to find complete collapse of data in stage 2 (see figure 13*b*) for six different situations.

The whistler tone value of St_b increases linearly with b; the slope of this line

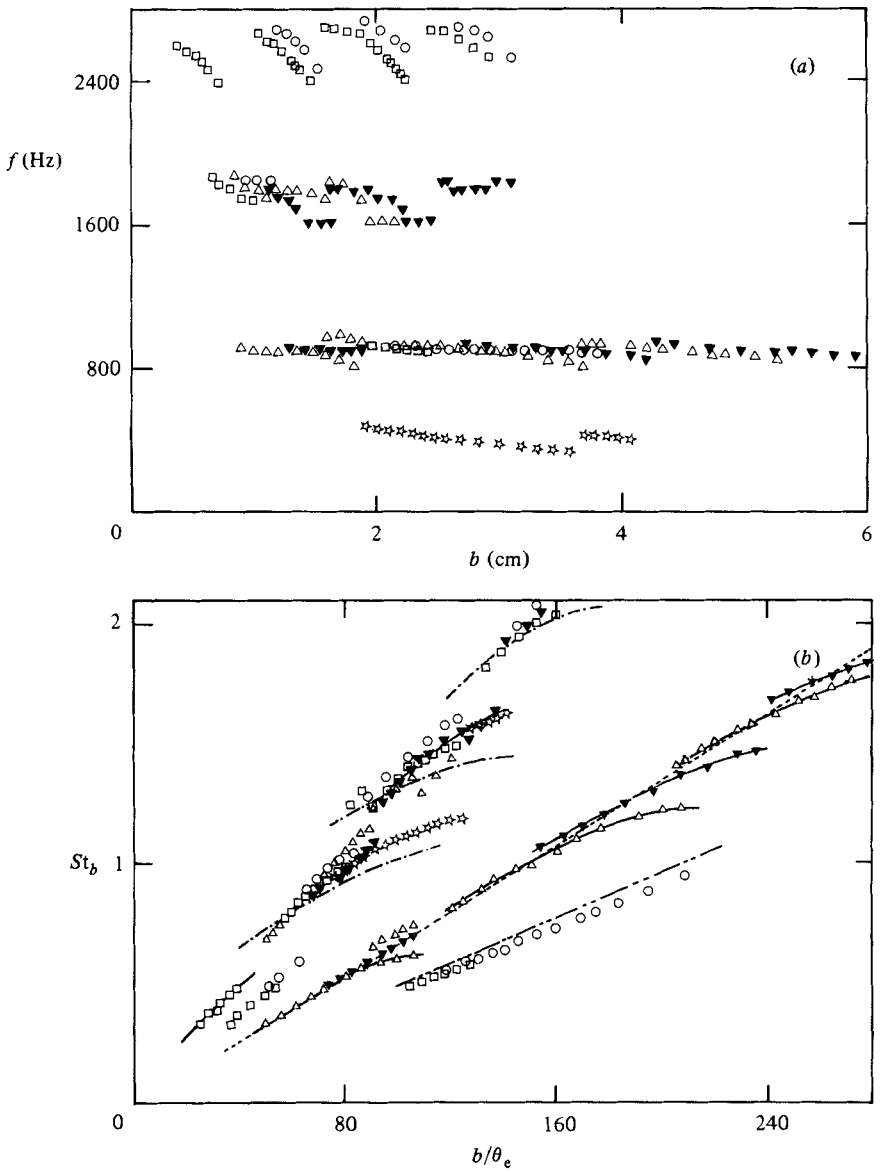

FIGURE 13. For caption see facing page.

decreases with increasing speed. Correspondingly, the $St_{\theta e}$ values are constant for each U_e, the constant value decreasing with increasing U_e.

Note that at $U_e = 10$ m s^{-1} there is a clear shear tone with the ring but none with the hole. This is to be expected because the sharper impinging edge of the ring should produce a stronger feedback. For this reason, $U_{e\,min}$ for the ring should be smaller than that for the hole; clearly, $U_{e\,min}$ for the ring is less than 10 m s^{-1}, while it is higher for the hole. There is no corresponding whistler tone at this speed because the ring-tone frequency is quite different from the corresponding whistler tone frequency. The b_{min} for the whistler tone with the ring is lower than that with the hole. This is again consistent with the expectation that the feedback from the ring is stronger and thus the tone should occur at a smaller b. Note that, at $U_e = 36$ m s^{-1}, there is even an earlier stage for the pipe–ring than for the pipe–hole.

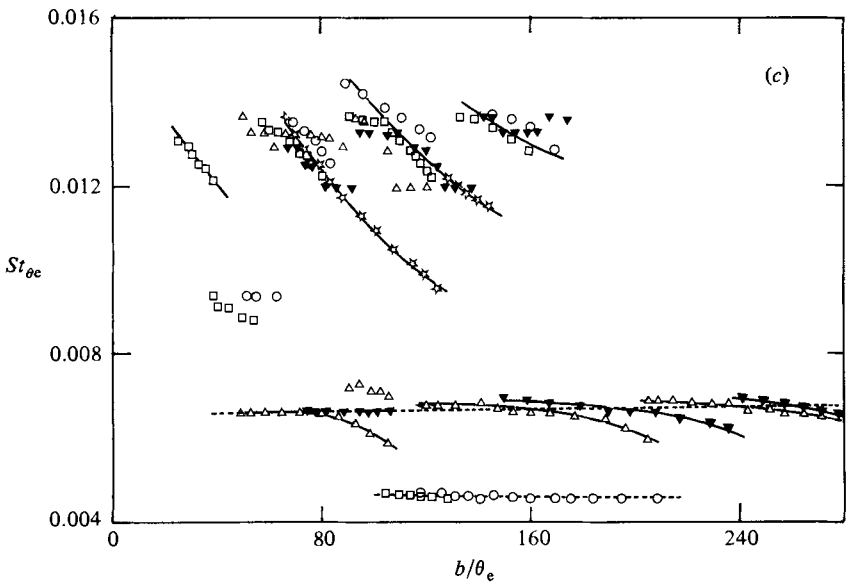

FIGURE 13. (*a*) Variation of frequency f with separation b for pipe–hole (PH) and pipe–ring (PR) configurations. The velocity (m s^{-1}) and the corresponding configuration are ☆, 10, PR; △, 24, PR; □, 36, PR; ▽, 24, PH; ○, 36 PH. (*b*) St_b *vs.* b/θ_e; legend as in (*a*): —·—·—, shear-layer tone (HZ); — - — - —, whistler tone with collar. (*c*) St_θ *vs.* b/θ_e; legend as in (*a*). The dotted straight lines denote $St_b \propto b$ or $St_{\theta e}$ = const. lines.

The shear-tone and whistler-tone amplitudes as functions of v are shown in figure 14(*a*) for $U_e = 24$ m s^{-1} and in figure 14(*b*) for $U_e = 36$ m s^{-1}. The shear-tone and whistler-tone stages occur fairly independently. At $U_e = 24$ m s^{-1}, the whistler-tone amplitude starts being smaller than the shear tone, but reaches rapidly a peak value significantly exceeding the latter. The increasing stages of both shear and whistler tones have decreasing peak amplitudes, because the feedback is weaker at larger L_c. The shear-tone and whistler-tone amplitudes are both higher for the ring, which is expected to produce a stronger feedback in comparison with that for the hole. Note that, at $U_e = 36$ m s^{-1}, the shear-tone and whistler-tone amplitudes are comparable. The whistler tone is considerably weaker at other values of b and the corresponding amplitudes are thus not shown.

3.10. *Comparison of whistler tone with pipe–ring and pipe–hole tones*

The pipe–ring and pipe–hole configurations were examined in order to obtain further support for the explanation proposed by us for the whistler-nozzle phenomenon. The data convincingly validate the explanation. Data in figure 12(*a*) for the whistler tone are consistent with those in figure 13(*b*) for the pipe–ring and pipe–hole systems; note the linear variations of St_c and St_b with L_c/θ_e and b/θ_e, respectively. For $U_e = 36$ m s^{-1}, these two variations are essentially identical; see comparison shown in figure 13(*b*). There is also a good agreement in the $St_{\theta e}$ values; for example, for a value of L_c/θ_e or b/θ_e of about 160, the $St_{\theta e}$ values are essentially identical. Similarly, the St_b values for the fundamental for $b/\theta_e \approx 200$ are essentially the same in figures 12(*a*) and 13(*b*). The departure from an exact linear variation in figure 12(*a*) and from a constant value in figure 12(*b*) is different from those for pipe–ring and pipe–hole systems. These differences are to be expected. With increasing collar length L_c, the effective length of the pipe also increases and hence the organ-pipe mode frequency decreases, while, in the case of the pipe–ring or pipe–hole, the organ-pipe

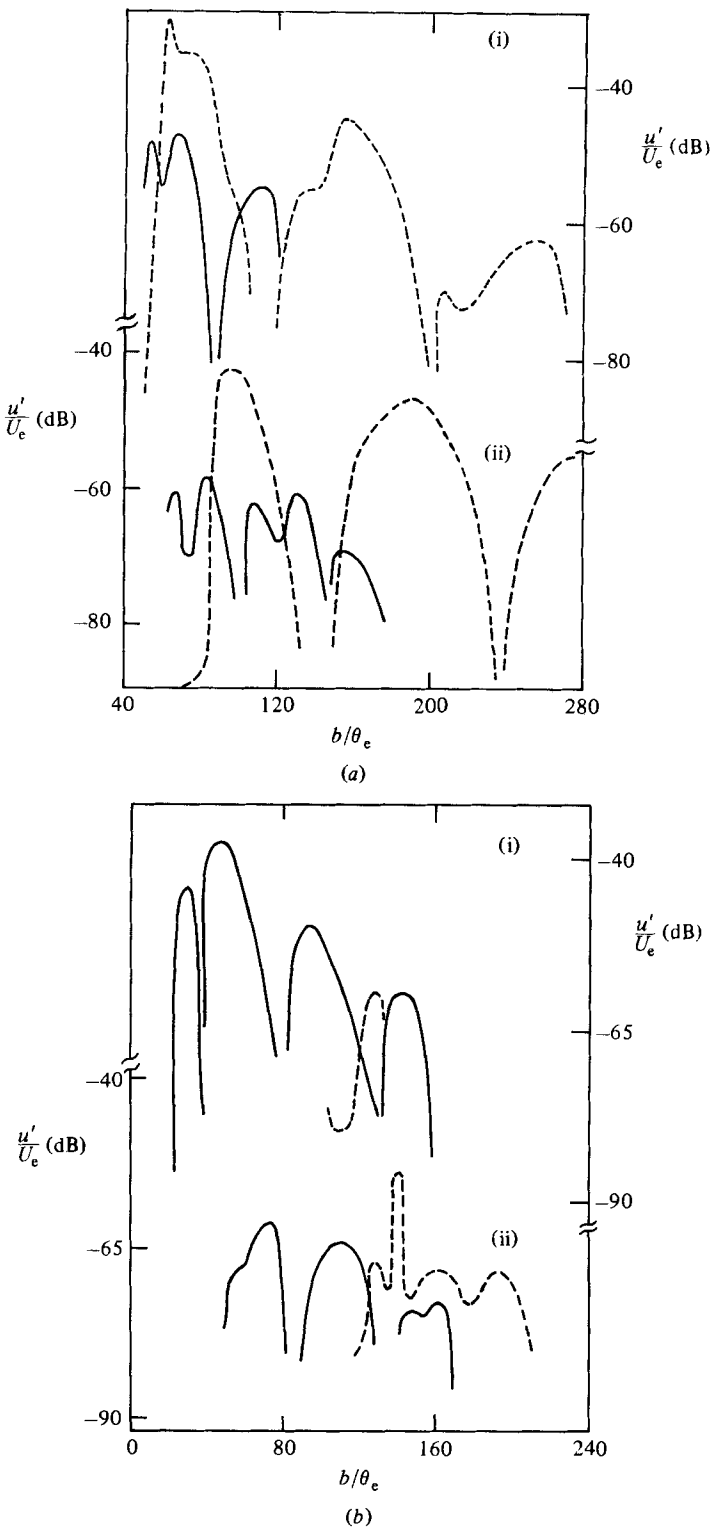

FIGURE 14. (*a*) Amplitude variation of whistler tone (dotted line) and shear tone (solid line) for $U_e = 24$ m s^{-1}, $L_p = 15.24$ cm, $D = 2.54$ cm: (i) pipe–ring; (ii) pipe–hole. (*b*) Amplitude variation of whistler tone (dotted line) and shear tone (solid line) for $U_e = 36$ m s^{-1}, $L_p = 15.24$ cm, $D = 2.54$ cm: (i) pipe–ring; (ii) pipe–hole.

D (cm)	L_p (cm)	U_e (m s^{-1})	St_D
2.54	15.24	36	0.58
	30.48	36	0.33
	60.96	36	0.37
7.62	30.48	36	0.8
	30.48	60	0.51
	60.96	36	0.51
3.81	5.08	127	0.52
	5.08	195	0.53
	10.16	86	0.52
	10.16	127	0.35
	15.24	86	0.38
	15.24	127	0.54
	15.24	195	0.43
	22.86	86	0.56
	30.48	86	0.6
	30.48	127	0.57
	30.48	195	0.42

TABLE 3. Approximate St_D values of the dominant mode of whistler excitation determined from far-field jet noise spectra

length and frequency remain unchanged. The comparatively worse collapse of the data with the collar is also to be expected. Since θ_e varies continuously with the collar length (see HH), the data would perhaps collapse better if the actual θ_e for each L_c were used. This would be prohibitively time-consuming and cumbersome because of the interference of the collar. That is why the θ_e values used in figures 12 (a, b) are the corresponding unexcited values.

The amplitudes reported in figures 6 and 14 cannot be directly compared because the sensor locations for the whistler nozzle and for the pipe–ring or pipe–hole had to be different. However, the audible tone was much louder for the whistler nozzle than for the pipe–ring or pipe–hole. This is because of the direct effect of the collar which enhances the flow surging and provides additional sound-radiating surfaces.

It should be emphasized that jet excitation is possible without the pipe–nozzle in ring-tone and hole-tone configurations if the initial condition is laminar. When initially turbulent, the pipe nozzle is essential for jet excitation. For initially turbulent shear layers at the exit of a contraction nozzle, self-excitation could not be induced.

Finally, it should be emphasized that the $St_{\theta e}$ values for the full-wave mode of whistler excitation fall in the range 0.009–0.012, representing the shear-layer tone (see HZ). However, the dominant mode (typically the half-wave mode) has a lower $St_{\theta e}$ (0.004–0.006). This paradox can be resolved by noting that the jet Strouhal number St_D ($= fD/U_e$) corresponding to the dominant mode nearly corresponds to the 'preferred mode' of the jet (Hussain & Zaman 1981). Table 3 presents approximate St_D values of the dominant whistler excitation for $D = 3.81$ cm at high subsonic velocities; the excitation frequencies were measured from jet noise in the far field with a condenser microphone. Note that the dominant St_D values for all the cases (except for $D = 7.62$ cm, $L_p = 30.48$ at $U_e = 36$ m s^{-1}) fall within 0.3–0.6. The case having a larger St_D (i.e. 0.8) has a weaker coupling (indicated by comparatively lower amplitude). Data in this table suggest that the 'preferred mode' of the jet plays a controlling role also; that is, the coupling of the two resonant mechanisms is tuned

to the 'preferred mode' of the jet. In essence, the whistler-nozzle phenomenon can be viewed as a coupling of three resonant mechanisms: the shear-layer tone, the organ-pipe resonance of the pipe nozzle and the 'preferred mode' of the jet.

This research was supported by NASA Lewis Research Center Grant NAG-3-198. The authors are grateful to Drs G. H. Koopman and D. Bechert for detailed discussions on the data and reviews of the manuscript.

REFERENCES

BRADSHAW, P., FERRISS, D. H. & JOHNSON, R. F. 1964 *J. Fluid Mech.* **19**, 591.

BROWN, G. B. 1937 *Proc. Phys. Soc. Lond.* **49**, 493.

CLARK, A. R. & HUSSAIN, A. K. M. F. 1979 In *Turbulent Shear Flows* (London), p. 2.30.

COLES, D. E. 1962 *Rand Corp. Rep.* R-403-PR.

CRIGHTON, D. & INNES, D. 1981 *AIAA Paper* 81-0061.

CROW, S. C. & CHAMPAGNE, F. H. 1971 *J. Fluid Mech.* **48**, 547.

CURLE, N. 1953 *Proc. R. Soc. Lond.* **A216**, 412.

HASAN, M. A. Z. & HUSSAIN, A. K. M. F. 1979 *J. Acoust. Soc. Am.* **65**, 1140.

HASAN, M. A. Z. & HUSSAIN, A. K. M. F. 1982 *J. Fluid Mech.* **115**, 59.

HILL, W. G. & GREENE, P. R. 1977 *Trans. ASME* I: *J. Fluids Engng* **99**, 520.

HO, C. & NOSSEIR, N. S. 1981 *J. Fluid Mech.* **195**, 119.

HUSAIN, Z. D. & HUSSAIN, A. K. M. F. 1979 *AIAA J.* **12**, 48.

HUSSAIN, A. K. M. F. 1981 In *The Role of Coherent Structures in Modelling Turbulence and Mixing* (ed. J. Jimenez). Lecture Notes in Physics, vol. 136, p. 252.

HUSSAIN, A. K. M. F. & CLARK, A. R. 1981 *J. Fluid Mech.* **104**, 263.

HUSSAIN, A. K. M. F. & ZAMAN, K. B. M. Q. 1975 In *Proc. 3rd Interagency Symp. on Univ. Res. in Transportation Noise, Univ. of Utah*, p. 314.

HUSSAIN, A. K. M. F. & ZAMAN, K. B. M. Q. 1978 *J. Fluid Mech.* **87**, 349.

HUSSAIN, A. K. M. F. & ZAMAN, K. B. M. Q. 1981 *J. Fluid Mech.* **110**, 39.

HUSSAIN, A. K. M. F. & ZAMAN, K. B. M. Q. 1982 *Univ. Houston Rep.* FM-14.

KARAMCHETI, K., BAUER, A. E., SHIELDS, W. L., STEGEN, G. R. & WOOLLEY, J. P. 1969 *NASA* SP-207, p. 207.

KIBENS, V. 1980 *AIAA J.* **18**, 434.

KINSLER, L. E. & FREY, A. R. 1962 *Fundamentals of Acoustics*. Wiley.

KNISELY, C. & ROCKWELL, D. 1981 *J. Fluid Mech.* **116**, 157.

KO, N. W. M. & DAVIES, P. O. A. L. 1971 *J. Fluid Mech.* **50**, 49.

LAU, J. C., FISHER, M. J. & FUCHS, H. V. 1972 *J. Sound Vib.* **22**, 379.

MICHALKE, A. 1965 *J. Fluid Mech.* **23**, 521.

PETERSEN, R. A. 1978 *J. Fluid Mech.* **89**, 469.

PFIZENMAIER, E. 1973 Doctor-Ingenieur thesis, Technische Universität Berlin.

POWELL, A. 1961 *J. Acoust. Soc. Am.* **33**, 4.

ROCKWELL, D. & NAUDASCHER, E. 1979 *Ann. Rev. Fluid Mech.* **11**, 67.

ROCKWELL, D. & SCHACHENMANN, A. 1982 *J. Fluid Mech.* **117**, 425.

SAROHIA, V. 1977 *AIAA J.* **15**, 984.

ZAMAN, K. B. M. Q. & HUSSAIN, A. K. M. F. 1980 *J. Fluid Mech.* **101**, 449.

ZIADA, S. & ROCKWELL, D. 1982 *J. Fluid Mech.* **118**, 79.